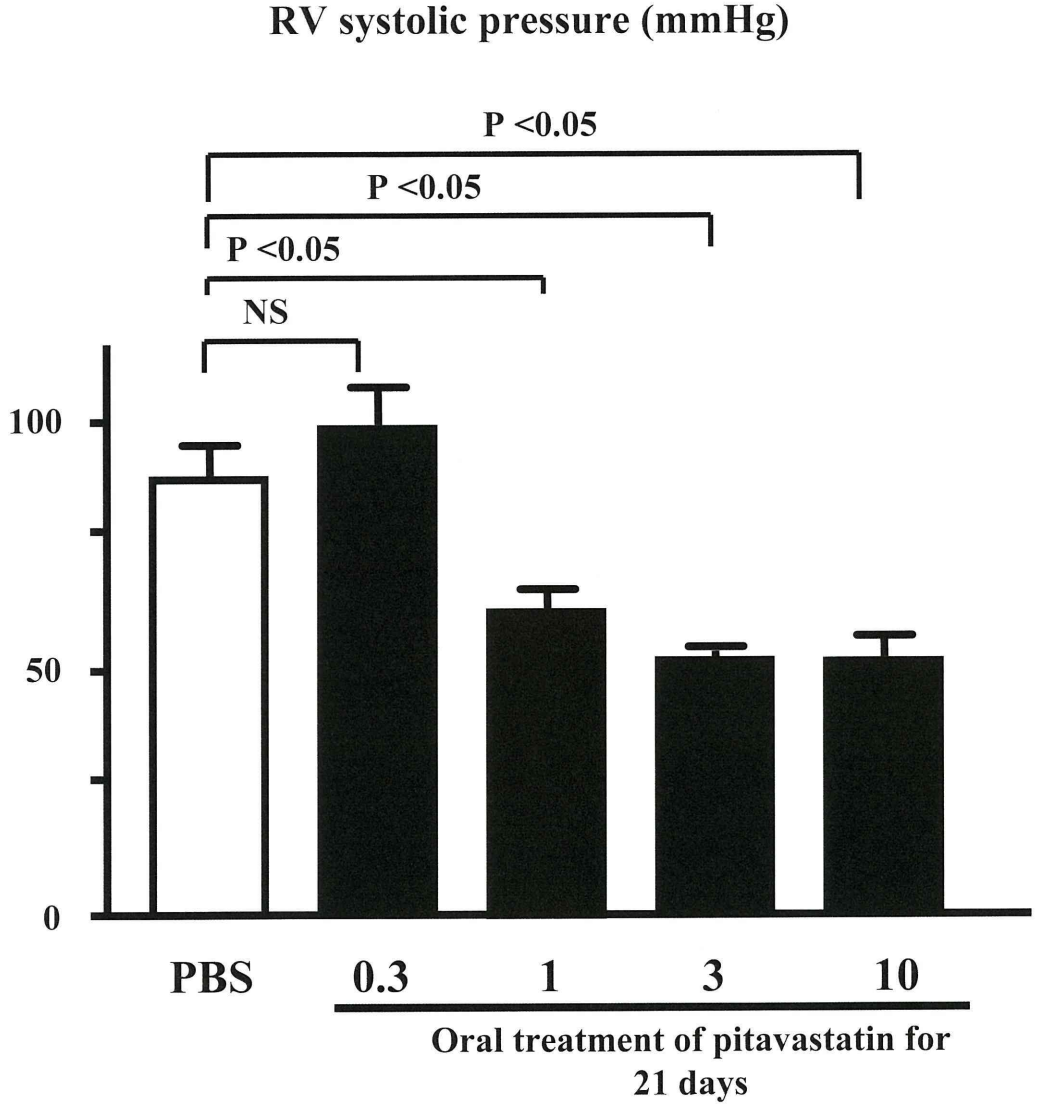

Figure S2. Effects of oral treatment of pitavastatin on right ventricular (RV) systolic pressure 3 weeks after MCT injection. Data are mean ± SEM ($n = 6$ each).

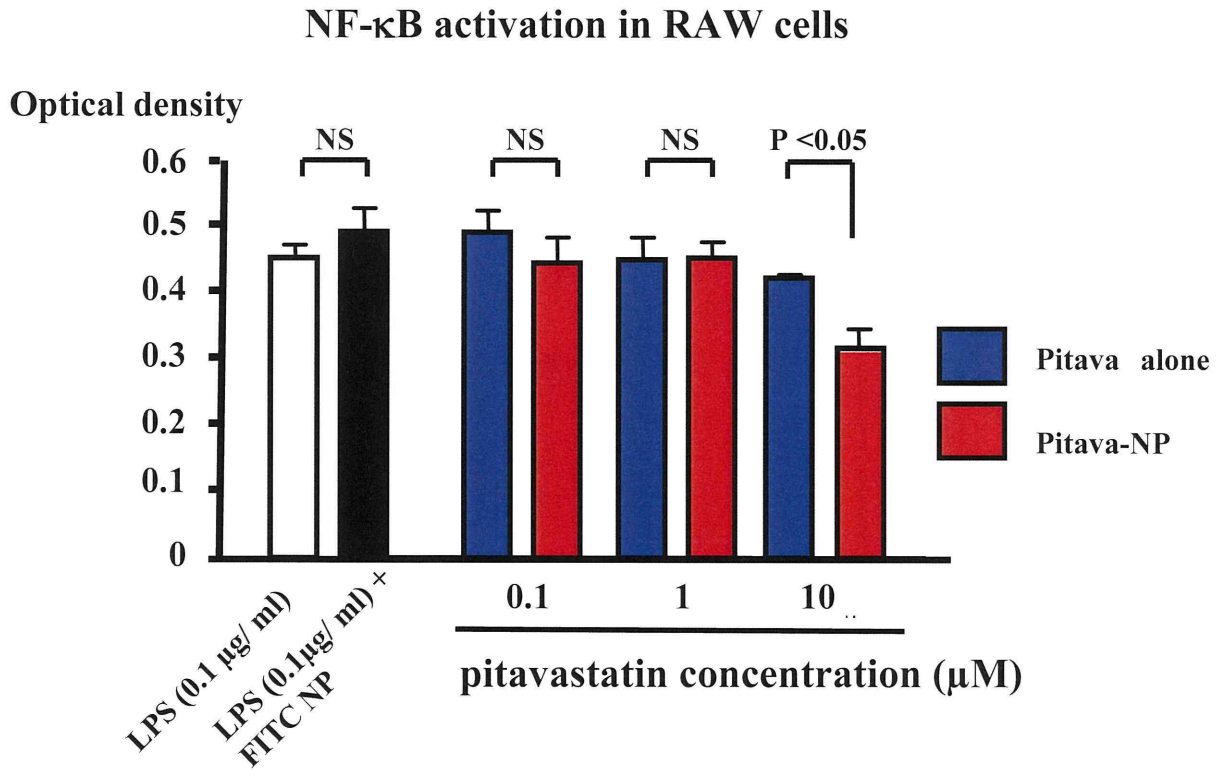

Figure S3 Effect of pitavastatin-NP on NF-κB activation of monocyte cell line (RAW cells)
Effects of pitavastatin-NP on LPS-stimulated activation of NF–κB (ELISA-based DNA binding assay against NF-kB p65 subunit: arbitrary unit). Data are mean ± SEM (*n*= 6 each).

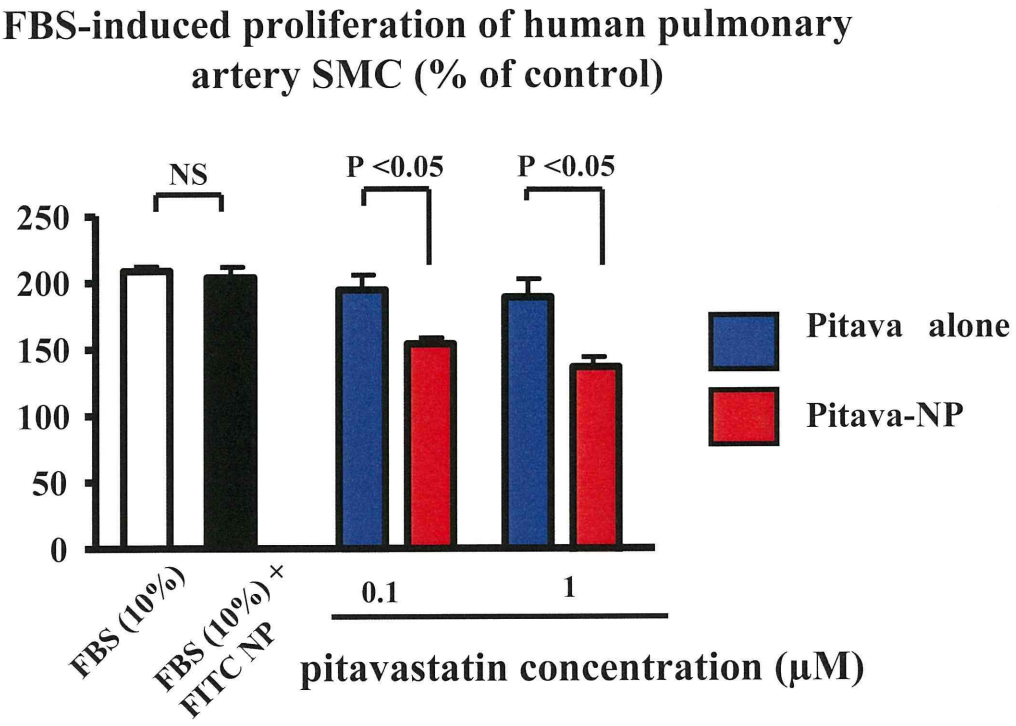

Figure S4. Effects of pitavastatin-NP versus pitavastatin on FBS-induced proliferation of human PASMCs (cell count per well). Data are mean ± SEM (n = 6 each).

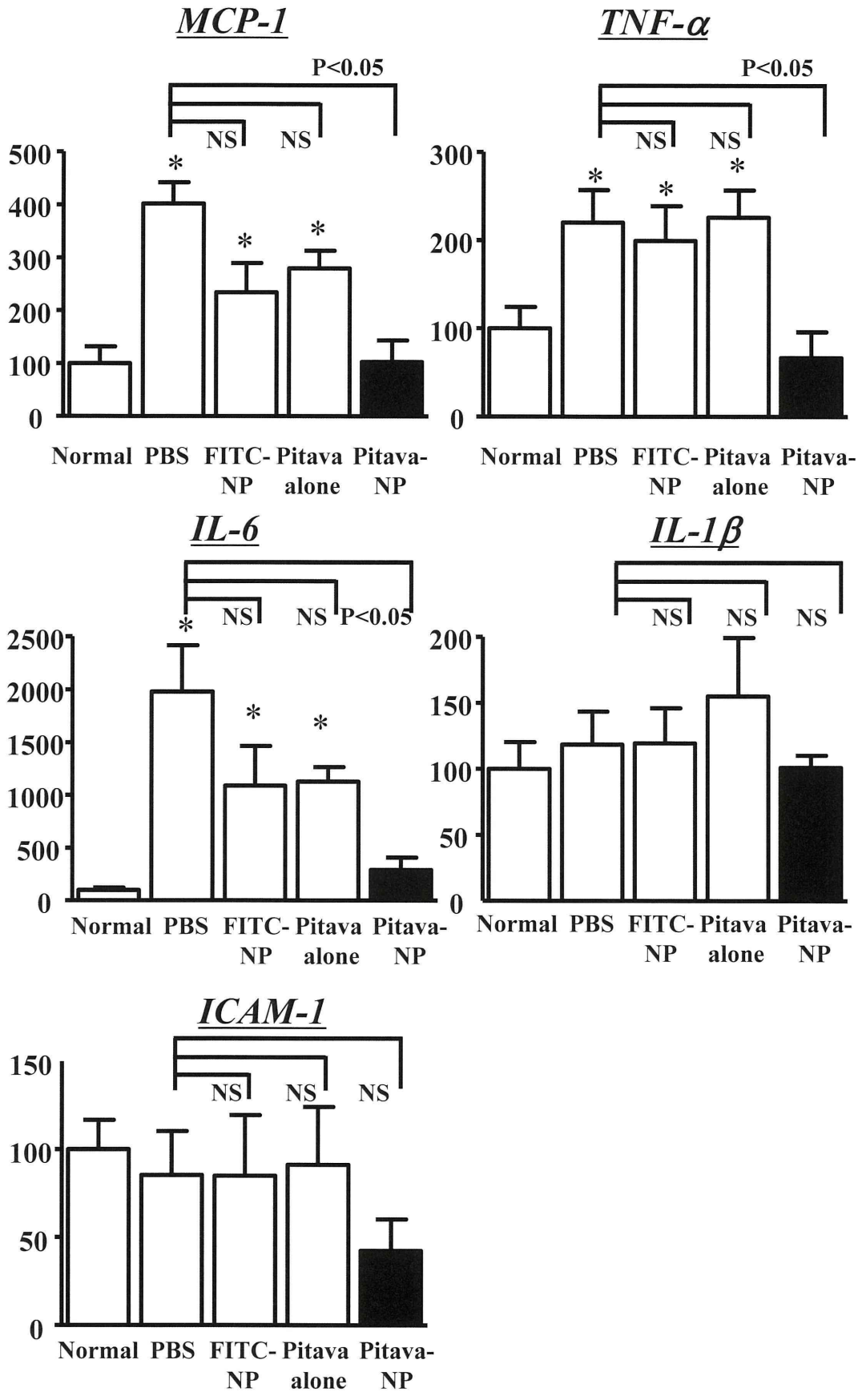

Figure S5. Effects of pitavastatin-NP on mRNA levels of various inflammatory and proliferative factors 21 days after MCT injection (n = 6 each). *$P < 0.05$ versus Normal. Data are mean ±SEM. NS; Not Significant.

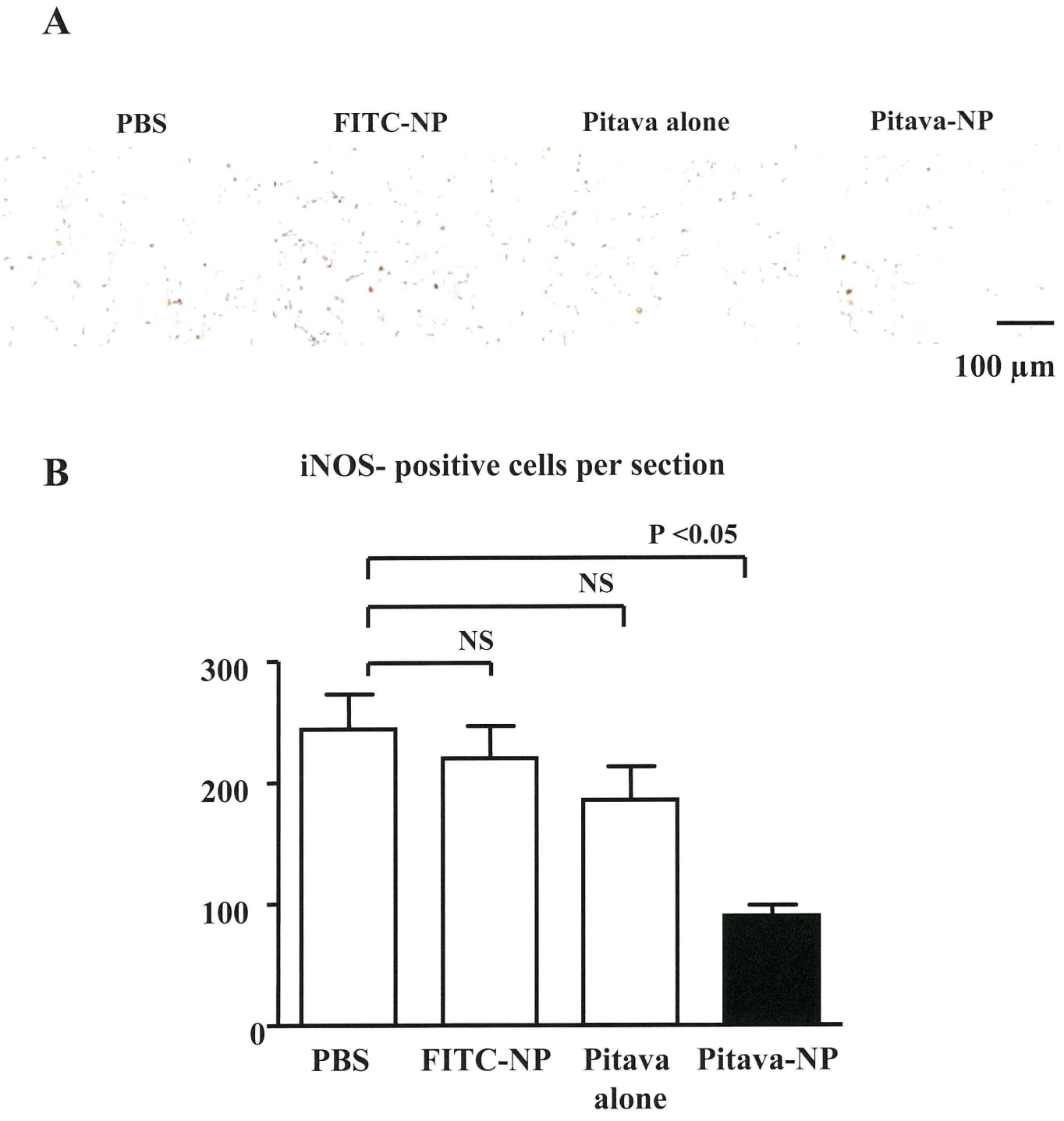

Figure S6. Effects of pitavastatin-NP on iNOS protein expression
A, Representative micrographs of lung tissues stained immunohistochemically for iNOS.
B, Effects of pitavastatin-NP on infiltration of iNOS-positive cells 21 days after MCT injection. Data are mean ±SEM (n = 6 each).

INTERNAL MEDICINE

□ CASE REPORT □

A Case of Multiple Focal Nodular Hyperplasia in the Liver Which Developed after Heart Transplantation

Takeo Fujino, Mari Nishizaka, Takeo Yufu and Kenji Sunagawa

Abstract

An 18-year-old woman, who had undergone cardiac allograft transplantation, developed continuous back pain two months after surgery. Abdominal computed tomography showed multiple enhanced lesions in her liver, which were not present before transplantation. One tumor bulged from the surface of the liver and compressed the stomach. Partial resection of the liver was performed and her symptoms improved. The pathological diagnosis was focal nodular hyperplasia (FNH). To our knowledge, this is the first report of multiple FNH after heart transplantation. Transplant clinicians may need to keep this possibility under consideration following heart transplantation.

Key words: heart transplantation, complications, multiple focal nodular hyperplasia

(Intern Med 50: 43-46, 2011)
(DOI: 10.2169/internalmedicine.50.4282)

Introduction

Focal nodular hyperplasia (FNH) is a benign liver tumor, which is often seen in young women. However, multiple FNH is rare. The pathogenesis of FNH is not well understood. There are many possible complications we should be aware of following heart transplantation. Here we present the first case, to our knowledge, of development of multiple FNH after heart transplantation. The current case is instructive and indicates that we should keep this possibility under consideration if new liver lesions were detected after heart transplantation.

Case Report

An 18-year-old female cardiac allograft recipient was referred to our hospital for suspected rejection six months after transplant. She underwent transplantation in January 2008 for uncontrollable right ventricular (functional left ventricular) dysfunction due to corrected transposition of the great arteries, status post Rastelli operation, tricuspid valve replacement, and cardiac resynchronization therapy (CRT). She had been taking oral contraceptives for about two years since menarche until heart transplantation to prevent anemia that could worsen heart failure. After the transplantation surgery, she started taking oral immunosuppressant agents including prednisolone 10 mg per day, mycophenolate mofetil 500 mg per day, and cyclosporine A, the trough concentration of which was regularly monitored to be maintained in the range of 160-240 ng/mL.

In March 2008 she developed continuous back pain. Osteoporotic bone disease was excluded. Steroid pulse therapy was given on suspicion of acute rejection, but her symptom did not improve. Therefore, in July, she was referred to our hospital for further investigation.

Physical examination did not show any abnormal findings, such as eczema, rush or abdominal pain. Her blood tests, chest X-ray, electrocardiogram, and cardiac echocardiography did not suggest the cause of her symptom. Cardiac catheterization revealed almost normal hemodynamics. Her coronary arteries were intact without any vasculopathy on coronary angiography and intravascular ultrasonography. Endomyocardial biopsy did not explain her symptom either with the tissue showing minimum cellular rejection Grade 1 R by Standardized Cardiac Biopsy Grading (1).

During her evaluation, abdominal computed tomography (CT) showed multiple enhanced lesions in the liver, which had not been seen prior to heart transplantation in March 2004 (Fig. 1A, 1B). Central scars were not apparent in the

Department of Cardiovascular Medicine, Kyushu University Hospital, Japan
Received for publication July 28, 2010; Accepted for publication September 17, 2010
Correspondence to Dr. Takeo Fujino, tafujino@cardiol.med.kyushu-u.ac.jp

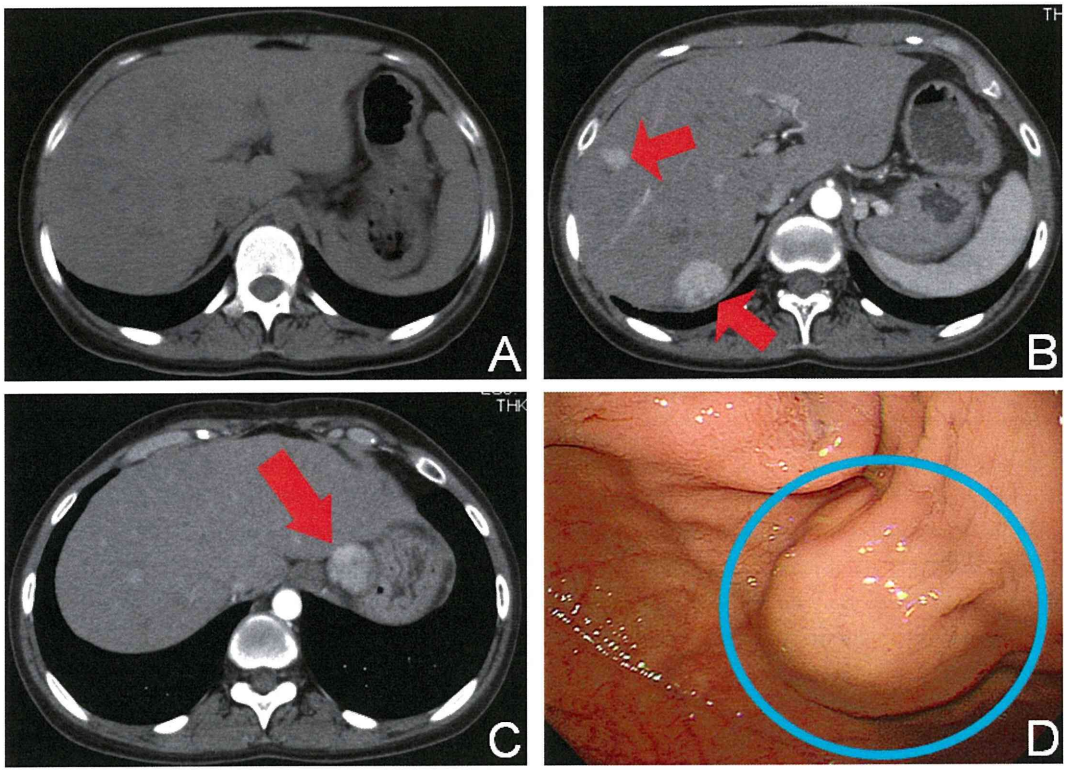

Figure 1. **A: Computed tomography of the liver did not show any distinct lesions four years before heart transplantation. B: Computed tomography showed multiple lesions (arrows) seven months after heart transplantation. C: Computed tomography showed a distinct tumor in the left lateral segment of the liver (arrow). D: Endoscopic findings of the stomach; the tumor bulged from the surface of the liver and compressed the stomach (circle).**

lesions. We considered magnetic resonance imaging (MRI), which is considered to be more informative for the differential diagnosis of liver tumors (2). However, as the leads of CRT-defibrillator (CRT-D) were still in her vein, MRI was not possible.

One tumor in the left lateral segment bulged from the surface of the liver and compressed the stomach (Fig. 1C, 1D). Since it was suspected to be related to her back pain and because there was fear of rupture and possible malignancy (including posttransplant lymphoproliferative disease), partial resection of the liver was performed in October 2008 (Fig. 2A, 2B). The pathological findings of the tumor included hyperplastic hepatocytes with acinar structure, ductular reaction, abnormal vessels, and central scar (Fig. 2C-F), which are typical findings of FNH. Her back discomfort improved after the surgery. In fact, even though the residual lesions are slowly enlarging, back pain remains absent about two years after surgery.

Discussion

There are many possible complications after heart transplantation, such as rejection, coronary vasculopathy, infection, and malignancy (3). We can never be too careful to notice any unusual symptoms or signs in transplant recipients, as they are often atypical presentations of these pathological complications. The present patient complained of continuous back pain. We considered the above possibilities and attempted to determine the cause of her complaint. In the process of her evaluation, many nodular lesions were detected in her liver, which had not been present before heart transplantation. The pathological diagnosis of the tumors was found to be FNH. After surgical resection, her back pain resolved. We presume, in the current case, FNH was related to her complaint.

FNH is one of the most common benign neoplasms of the liver, which accounts for 8% of all primary hepatic tumors. It is more commonly found in women (4). In most cases it appears solitary. Multiple FNH is extremely rare, and few reports exist in the literature (5). The pathogenesis of multiple FNH is not well understood. In the current case, the etiology of the multiple FNH cannot be definitively attributed to her prior heart transplantation. Other possible contributing factors present before and after transplantation, including the use of oral contraceptives, surgical stress, and immunosuppressant therapy.

A possible relation between FNH and oral contraceptive use has been proposed but remains controversial (6). In the current case, the recipient had been taking oral contraceptives for about two years since menarche preceding heart transplantation to prevent anemia, which may have contributed to the development of multiple FNH. Because candi-

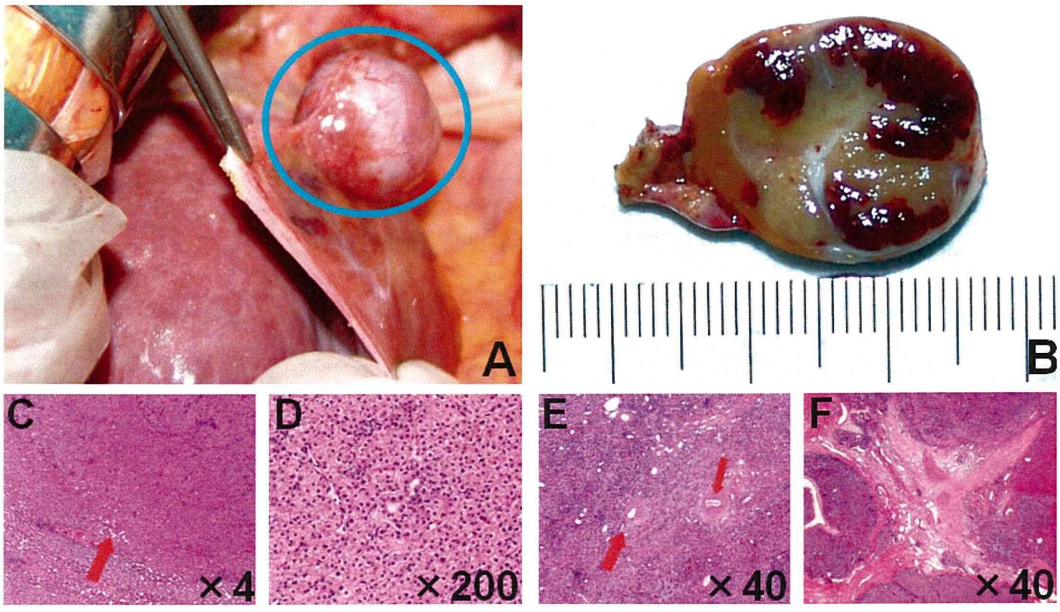

Figure 2. **Intraoperative findings of the tumor. A: A distinct tumor in the left lateral segment bulged from the surface of the liver (circle). It was round with a smooth surface, and the texture was elastic and hard. B: The surface of the tumor was encased by a membranous layer, and the section of the tumor showed well-demarcated lesions inside. The tumor was 2.5×2.5 cm in size. C-F: Microscopic sections of the tumor (Hematoxylin and Eosin staining). C and D show hyperplastic hepatocytes (arrows). E shows abnormal vessels (arrows). F shows central scar of the tumor. They are typical findings of focal nodular hyperplasia.**

dates for heart transplantation suffer from severe heart failure, it is not unusual to receive oral contraceptives to prevent anemia or pregnancy. The current report suggests that development of FNH should be especially considered in such patients.

There is no evidence for the relationship between immunosuppressants and FNH, but immunosuppressant agents are causally related to malignant tumors, including post-transplant lymphoproliferative disease (7). The current patient needs to continue immunosuppressant therapy. With no evidence for rejection having been seen during periodic cardiac biopsy, we have been modulating her agents carefully. In fact, the residual lesions are slowly enlarging after surgery, but surgical resection of the liver for treatment of FNH is not indicated unless the patient has symptoms related to the tumor size or location (4). Our clinical plan includes periodic abdominal CT in order to monitor the residual tumors.

In this case we diagnosed FNH by tissue pathology, but, in general, diagnosis by imaging is preferred. For non-invasive diagnosis, MRI is more useful than CT, the sensitivity and specificity of which are 70% and 98%, respectively (2). The patient, however, could not undergo MRI because CRT-D leads were still in her vein. In addition, because one tumor was suspected of causing her back pain and because of risk of rupture, we chose prompt surgical resection.

Again, the causality cannot be proven. However, this is an instructive case; the first case report, to our knowledge, of multiple FNH observed after heart transplantation, although FNH is not rare after hematopoietic stem cell transplantation (8). To the best of our knowledge, there are no case reports of FNH after solid organ transplantation. Data of Japanese patients after heart transplantation are scarce, and accumulation of such data will be clinically useful. Based on the present report, we suggest that multiple FNH should be considered if new liver lesions are detected after heart transplantation, especially if the patient had taken oral contraceptives before surgery.

The authors state that they have no Conflict of Interest (COI).

References

1. Stewart S, Winters GL, Fishbein MC, et al. Revision of the 1990 working formulation for the standardization of nomenclature in the diagnosis of heart rejection. J Heart Lung Transplant **24**: 1710-1720, 2005.
2. Vilgrain V. Focal nodular hyperplasia. Eur J Radiol **58**: 236-245, 2006.
3. Tjang YS, van der Heijden GJ, Tenderich G, Grobbee DE, Korfer R. Survival analysis in heart transplantation: results from an analysis of 1290 cases in a single center. Eur J Cardiothorac Surg **33**: 856-861, 2008.
4. Bonney GK, Gomez D, Al-Mukhtar A, Toogood GJ, Lodge PA, Prasad R. Indication for treatment and long-term outcome of focal nodular hyperplasia. HPB (Oxford) **9**: 368-372, 2007.
5. Kim J, Nikiforov YE, Moulton JS, Lowy AM. Multiple focal nodular hyperplasia of the liver in a 21-year-old woman. J Gastrointest Surg **8**: 591-595, 2004.

6. Giannitrapani L, Soresi M, La Spada E, Cervello M, D'Alessandro N, Montalto G. Sex hormones and risk of liver tumor. Ann N Y Acad Sci **1089**: 228-236, 2006.
7. Zafar SY, Howell DN, Gockerman JP. Malignancy after solid organ transplantation: an overview. Oncologist **13**: 769-778, 2008.
8. Suduour H, Mainard L, Baumann C, Clement L, Salmon A, Bordigoni P. Focal nodular hyperplasia of the liver following hematopoietic SCT. Bone Marrow Transplant **43**: 127-132, 2009.

Am J Physiol Regul Integr Comp Physiol 300: R155–R165, 2011.
First published November 3, 2010; doi:10.1152/ajpregu.00540.2010.

Dynamic characteristics of baroreflex neural and peripheral arcs are preserved in spontaneously hypertensive rats

Toru Kawada,[1] Shuji Shimizu,[1,2] Atsunori Kamiya,[1] Yusuke Sata,[1] Kazunori Uemura,[1] and Masaru Sugimachi[1]

[1]*Department of Cardiovascular Dynamics, National Cerebral and Cardiovascular Center Research Institute, Osaka, Japan; and* [2]*Japan Association for the Advancement of Medical Equipment, Tokyo, Japan*

Submitted 18 August 2010; accepted in final form 3 November 2010

Kawada T, Shimizu S, Kamiya A, Sata Y, Uemura K, Sugimachi M. Dynamic characteristics of baroreflex neural and peripheral arcs are preserved in spontaneously hypertensive rats. *Am J Physiol Regul Integr Comp Physiol* 300: R155–R165, 2011. First published November 3, 2010; doi:10.1152/ajpregu.00540.2010.—Although baroreceptors are known to reset to operate in a higher pressure range in spontaneously hypertensive rats (SHR), the total profile of dynamic arterial pressure (AP) regulation remains to be clarified. We estimated open-loop transfer functions of the carotid sinus baroreflex in SHR and Wistar Kyoto (WKY) rats. Mean input pressures were set at 120 (WKY_{120} and SHR_{120}) and 160 mmHg (SHR_{160}). The neural arc transfer function from carotid sinus pressure to efferent splanchnic sympathetic nerve activity (SNA) revealed derivative characteristics in both WKY and SHR. The slope of dynamic gain (in decibels per decade) between 0.1 and 1 Hz was not different between WKY_{120} (10.1 ± 1.0) and SHR_{120} (10.4 ± 1.1) but was significantly greater in SHR_{160} (13.2 ± 0.8, $P < 0.05$ with Bonferroni correction) than in SHR_{120}. The peripheral arc transfer function from SNA to AP showed low-pass characteristics. The slope of dynamic gain (in decibels per decade) did not differ between WKY_{120} (-34.0 ± 1.2) and SHR_{120} (-31.4 ± 1.0) or between SHR_{120} and SHR_{160} (-32.8 ± 1.3). The total baroreflex showed low-pass characteristics and the dynamic gain at 0.01 Hz did not differ between WKY_{120} (0.91 ± 0.08) and SHR_{120} (0.84 ± 0.13) or between SHR_{120} and SHR_{160} (0.83 ± 0.11). In both WKY and SHR, the declining slope of dynamic gain was significantly gentler for the total baroreflex than for the peripheral arc, suggesting improved dynamic AP response in the total baroreflex. In conclusion, the dynamic characteristics of AP regulation by the carotid sinus baroreflex were well preserved in SHR despite significantly higher mean AP.

systems analysis; transfer function; white noise; sympathetic nerve activity; arterial pressure

THE ARTERIAL BAROREFLEX IS an important negative feedback system that stabilizes systemic arterial pressure (AP) against exogenous disturbances in daily activities. The sympathetic limb of the arterial baroreflex system may be analyzed by dividing it into two principal subsystems (23). One is a controller subsystem that describes the relationship between baroreceptor pressure input and efferent sympathetic nerve activity (SNA). The other is an effector subsystem that describes the relationship between SNA and AP. Hereafter, in this article, we refer to the former as the neural arc and the latter as the peripheral arc (9). In normal physiological conditions, changes in AP affect SNA via the neural arc, and the changes in SNA, in turn, affect AP via the peripheral arc. This closed-loop operation makes it difficult to identify the dynamic characteristics of the neural and peripheral arcs separately (see APPENDIX) (18). To circumvent the closed-loop problem, the carotid sinus baroreceptor regions were isolated from the systemic circulation, and open-loop transfer function analyses were performed in anesthetized rabbits (9) and rats (31). In both species, the neural arc revealed "derivative" characteristics, which means that the dynamic gain of the SNA response becomes greater as the frequency of modulation increases. In contrast, the peripheral arc showed "low-pass" characteristics, which means that the dynamic gain of the AP response becomes smaller as the frequency of modulation increases. It has been interpreted that the fast neural arc partially compensates for the slow peripheral arc to improve the speed of response of the total baroreflex system (9).

In chronic hypertension, the arterial baroreflex is reset to operate in a higher pressure range (2). Both carotid sinus (24) and aortic baroreceptors (30) show the resetting in spontaneously hypertensive rats (SHR). Although changes in vascular properties induced by sustained hypertension, such as reduced distensibility, may decrease the baroreflex sensitivity, the dynamic characteristics of AP regulation by the arterial baroreflex in hypertension are not fully understood. In a previous study, Harada et al. (7) have shown that the baroreflex neural arc retains its derivative characteristics in SHR. Since they perturbed AP by aortic balloon inflation and deflation, they were unable to quantify the dynamic AP response to changes in SNA (i.e., the peripheral arc). As a result, the total profile of the dynamic AP regulation in SHR remains to be clarified. The aim of the present study was to comprehensively identify the dynamic characteristics of the neural arc, peripheral arc, and total baroreflex in SHR and compare them with those estimated in normotensive Wistar Kyoto rats (WKY).

MATERIALS AND METHODS

Animals were cared for in strict accordance with the Guiding Principles for the Care and Use of Animals in the Field of Physiological Sciences, which has been approved by the Physiological Society of Japan. All experimental protocols were reviewed and approved by the Animal Subjects Committee at the National Cerebral and Cardiovascular Center.

Surgical preparation. Main experiments were performed in age-matched male WKY ($n = 7$, 21.6 ± 3.7 wk) and SHR ($n = 6$, 22.2 ± 4.5 wk). Each rat was anesthetized with an intraperitoneal injection (2 ml/kg) of a mixture of urethane (250 mg/ml) and α-chloralose (40 mg/ml), and mechanically ventilated with oxygen-enriched room air. A venous catheter was inserted into the right femoral vein, and the above anesthetic mixture, diluted 20-fold, was administered continuously (2–3 $ml \cdot kg^{-1} \cdot h^{-1}$). An arterial catheter was inserted into the right femoral artery to measure AP. Heart rate (HR) was obtained

Address for reprint requests and other correspondence: T. Kawada, Dept. of Cardiovascular Dynamics, National Cerebral and Cardiovascular Center Research Institute, 5-7-1 Fujishirodai, Suita, Osaka 565–8565, Japan (e-mail: torukawa@res.ncvc.go.jp).

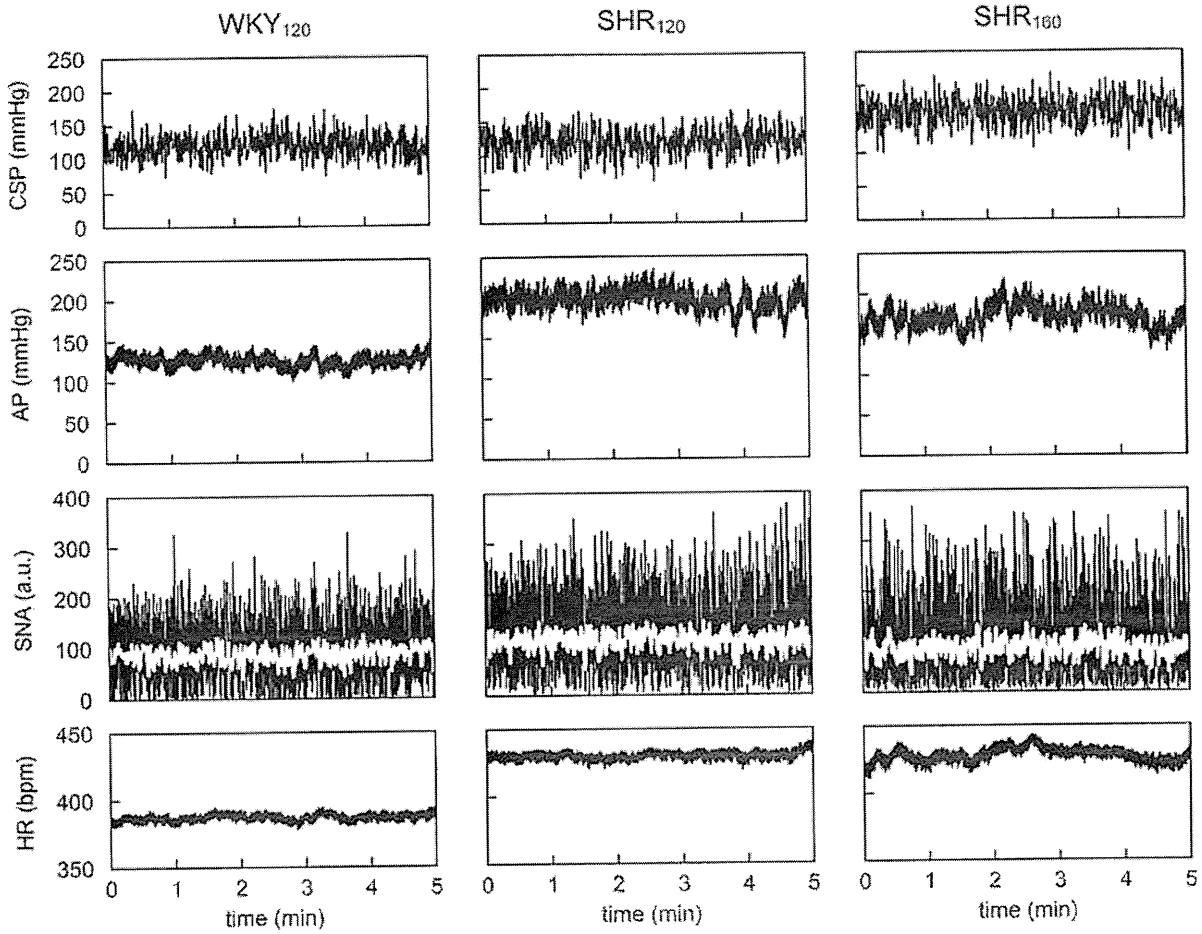

Fig. 1. Typical recordings of carotid sinus pressure (CSP), arterial pressure (AP), sympathetic nerve activity (SNA), and heart rate (HR) obtained from a Wistar Kyoto (WKY) rat and a spontaneously hypertensive rat (SHR). CSP was perturbed according to a Gaussian white noise with mean input pressure of 120 mmHg (WKY_{120} and SHR_{120}) or 160 mmHg (SHR_{160}). White lines in the SNA data indicate 2-s moving average SNA signals.

from AP through a cardiotachometer. Another venous catheter was inserted into the left femoral vein to infuse Ringer solution (6 $ml \cdot kg^{-1} \cdot h^{-1}$).

A postganglionic branch from the splanchnic sympathetic nerve was exposed through a left flank incision and a pair of stainless-steel wire electrodes (Bioflex wire AS633; Cooner Wire, Chatsworth, CA) was attached to record SNA. The nerve and electrodes were covered with silicone glue (Kwik-Sil; World Precision Instruments, Sarasota, FL, USA) for insulation and fixation. To quantify the nerve activity, the preamplified nerve signal was band-pass filtered at 150–1,000 Hz, and then full-wave rectified and low-pass filtered with a cut-off frequency of 30 Hz. Pancuronium bromide (0.4 $mg \cdot kg^{-1} \cdot h^{-1}$) was administered to prevent muscular activity from contaminating the SNA recording. At the end of the experiment, we confirmed the disappearance of SNA after an intravenous bolus injection of a ganglionic blocker hexamethonium bromide (60 mg/kg) and recorded the noise level.

Table 1. *Mean arterial pressure, heart rate, and sympathetic nerve activity during dynamic input protocol*

	WKY_{120}	SHR_{120}	SHR_{160}
Mean AP, mmHg	105 ± 5	176 ± 17**	143 ± 14†
Mean HR, bpm	406 ± 18	432 ± 19	423 ± 15
Mean SNA, au	85 ± 12	147 ± 15*	110 ± 15†

Data are presented in means ± SE values [$n = 7$ for Wistar-Kyoto (WKY) and $n = 6$ for spontaneously hypertensive rats (SHR)]. AP, arterial pressure; HR, heart rate; SNA, sympathetic nerve activity; bpm, beats per minute; au, arbitrary unit. *$P < 0.05$ and **$P < 0.01$, WKY_{120} vs. SHR_{120} by unpaired-t-test with Bonferroni correction. †$P < 0.05$, SHR_{120} vs. SHR_{160} by paired-t-test with Bonferroni correction.

Bilateral vagal and aortic depressor nerves were sectioned at the neck to avoid reflexes from the cardiopulmonary region and aortic arch. The carotid sinus regions were isolated from the systemic circulation using previously reported procedures (32, 34) with modifications. Briefly, a 7–0 polypropylene suture with a fine needle (PROLENE; Ethicon, Cornelia, GA) was passed through the tissue between the external and internal carotid arteries, and the external carotid artery was ligated close to the carotid bifurcation. The internal carotid artery was embolized by injecting two to three steel balls (0.8 mm in diameter; Tsubaki Nakashima, Nara, Japan) from the common carotid artery. The isolated carotid sinuses were filled with warmed Ringer solution through catheters inserted into the common carotid arteries. The carotid sinus pressure (CSP) was controlled using a servo-controlled piston pump. Heparin sodium (100 U/kg) was given intravenously to prevent blood coagulation. Body temperature was maintained at ~38°C with a heating pad.

Protocols. Some animals showed deterioration of baroreflex responses soon after the completion of the surgical preparation, possibly due to the surgical damage to the carotid sinus nerves or the low brain

perfusion after bilateral common carotid occlusion. The baroreflex study described below was conducted only in animals showing persistent baroreflex-mediated SNA, AP, and HR responses for more than 30 min after completion of the surgical preparation.

To estimate dynamic characteristics of the carotid sinus baroreflex, CSP was perturbed for 20 min using a Gaussian white noise (GWN) signal with a standard deviation of 20 mmHg (11, 12). The whiteness of the input is essential to estimate the system characteristics stably over a frequency range of interest (see APPENDIX). The mean input CSP was set at 120 mmHg in WKY (WKY_{120}) and SHR (SHR_{120}). Taking into account a priori knowledge that the baroreceptor is reset to a higher pressure range in SHR (2, 24), the same rats in SHR_{120} were also tested at a mean input CSP of 160 mmHg (SHR_{160}). The switching interval of GWN was 500 ms. The resulting input power spectral density was relatively constant up to 1 Hz, which was expected to cover the upper frequency range of interest with respect to the sympathetic arterial baroreflex in rats (31).

A supplemental protocol was performed in an additional three 18-wk-old male WKY rats to test the effect of changing the mean input CSP on the transfer function estimation. The GWN input was applied with the mean CSP set at 120 mmHg ($WKY_{120\text{-}S}$) and 160 mmHg ($WKY_{160\text{-}S}$). Six data sets were analyzed by acquiring two data sets from each rat using GWN signals of different sequences.

Data analysis. Data were sampled at 200 Hz using a 16-bit analog-to-digital converter and stored in a dedicated laboratory computer system. Dynamic characteristics of the baroreflex neural arc, peripheral arc, total baroreflex, and HR control were estimated by a standard open-loop transfer function analysis (see APPENDIX) (20). Data analysis was started from 120 s after initiation of the GWN input. The input-output data pairs were resampled at 10 Hz, and 12 segments were processed using 50%-overlapping bins of 1,024 points each.

To facilitate understanding of the transfer function, the step response corresponding to the transfer function was calculated as follows. A system impulse response was derived from the inverse Fourier transform of the transfer function. The step response was then obtained from the time integral of the impulse response.

Because the magnitude of SNA varied among animals depending on the recording conditions, SNA was normalized in each animal by assigning unity to the mean dynamic gain for frequencies below 0.03 Hz in the neural arc transfer function, for WKY_{120} and SHR_{120}. The following parameters of the transfer functions were compared: dynamic gain values at 0.01, 0.1, and 1 Hz ($G_{0.01}$, $G_{0.1}$, and G_1), and the slope of dynamic gain (G_{slope}) for the frequency range of 0.1 to 1 Hz. G_{slope} was calculated by a regression analysis between log frequency and log dynamic gain. For step response analysis of the neural arc, the negative peak response (S_{peak}), time to the negative peak (T_{peak}), and step response at 10 s (S_{10}) were calculated. For step response analyses of the peripheral arc, total baroreflex, and HR control, the steady-state response at 50 s (S_{50}) and initial slope (S_{slope}) were calculated. To calculate S_{slope}, a threshold value was determined at 5% S_{50}, and the

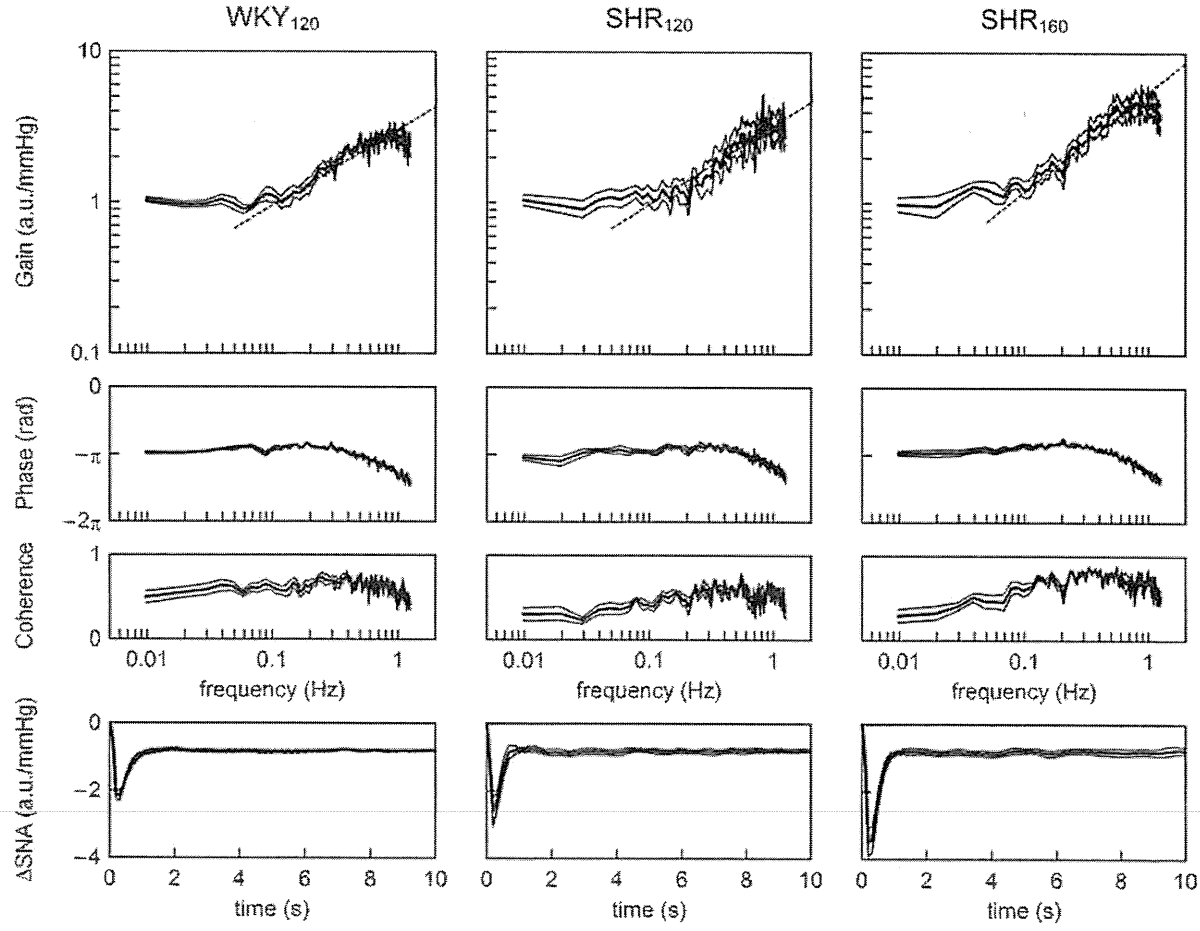

Fig. 2. Transfer functions of the baroreflex neural arc from CSP to SNA averaged for WKY_{120}, SHR_{120}, and SHR_{160} groups. Gain, phase, and coherence plots are shown. In the gain plots, the dashed oblique line indicates the mean slope of the dynamic gain (G_{slope}) estimated in the frequency range from 0.1 to 1 Hz. G_{slope} is significantly steeper in SHR_{160} than in SHR_{120}. *Bottom*: step responses of SNA calculated from the corresponding neural arc transfer functions. The peak response (S_{peak}) is significantly more negative in SHR_{160} than in SHR_{120}. In all panels, the bold and thin lines indicate mean and mean ± SE values, respectively.

first data point that exceeded the threshold was obtained. Starting from this first data point, a regression analysis was repeated while increasing the number of data points for the regression. The steepest slope thus obtained was defined as S_{slope}.

Statistical analysis. All data are presented as means ± SE. Differences between WKY_{120} and SHR_{120} were tested using unpaired *t*-test. Differences between SHR_{120} and SHR_{160} were tested using paired *t*-test. Taking into account the duplicated comparisons of the SHR_{120} data, differences between groups were considered to be significant when $P < 0.05$ with Bonferroni correction (i.e., $P < 0.025$ and $P < 0.005$ were interpreted as $P < 0.05$ and $P < 0.01$, respectively) (5). In the supplemental protocol, parameters were compared between $WKY_{120\text{-}S}$ and $WKY_{160\text{-}S}$ using paired *t*-test.

RESULTS

Figure 1 shows the typical experimental data obtained from an individual rat in the WKY_{120}, SHR_{120}, and SHR_{160} groups. The SHR_{120} and SHR_{160} data were derived from the same animal. In each group, CSP was perturbed according to a GWN signal, which caused variations in AP, SNA, and HR. The mean AP was significantly higher in SHR_{120} than in WKY_{120}, confirming hypertension in SHR (Table 1). The mean AP was significantly lower in SHR_{160} than in SHR_{120}, indicating that increasing the mean CSP enabled the reduction of the mean AP in SHR. The white lines in the SNA plots indicate 2-s moving average signals. Although mean SNA was higher in SHR_{120} than in WKY_{120}, this comparison could be influenced by the normalization of SNA. The mean SNA in SHR_{160} decreased significantly to 74 ± 6% of that in SHR_{120}. Although changes in mean HR appeared to parallel the changes in mean AP, there were no significant changes across the groups (Table 1).

The neural arc transfer functions averaged from the WKY_{120}, SHR_{120}, and SHR_{160} groups are shown in Fig. 2. In the gain plots, $G_{0.01}$ approximated unity in WKY_{120} and SHR_{120} because of the normalization procedure (Table 2). The dynamic gain became greater as the frequency increased above 0.1 Hz. There were no significant differences in $G_{0.1}$, G_1, and G_{slope} between WKY_{120} and SHR_{120}. $G_{0.01}$ also approximated unity in SHR_{160}, although SNA was normalized by the same normalization factor used for the SHR_{120} data. While $G_{0.1}$ did not differ significantly between SHR_{120} and SHR_{160}, G_1 and G_{slope} were significantly greater in SHR_{160}. The phase plots of three groups were similar: the phase was close to $-\pi$ radians at 0.01 Hz, deviated slightly toward 0 radians until 0.5 Hz, and then delayed beyond $-\pi$ radians as the frequency increased above 0.7 Hz. For the step responses, S_{10} and T_{peak} did not differ between WKY_{120} and SHR_{120} or between SHR_{120} and SHR_{160}. S_{peak} was not significantly different between WKY_{120} and SHR_{120} but was significantly more negative in SHR_{160} than in SHR_{120}.

The peripheral arc transfer functions averaged from the WKY_{120}, SHR_{120}, and SHR_{160} groups are shown in Fig. 3. In the gain plots, the dynamic gain became smaller, as the frequency increased above 0.05 Hz. $G_{0.01}$, $G_{0.1}$, G_1, and G_{slope} did not differ significantly between WKY_{120} and SHR_{120} or between SHR_{120} and SHR_{160} (Table 2). The phase plots of three groups were similar: the phase approached 0 radians at 0.01 Hz and was delayed by -2π radians as the frequency increased to 1 Hz. For the step responses, S_{50} and S_{slope} did not differ between WKY_{120} and SHR_{120} or between SHR_{120} and SHR_{160}.

Table 2. *Parameters of estimated transfer functions and step responses*

	WKY_{120}	SHR_{120}	SHR_{160}
Neural arc			
$G_{0.01}$, au/mmHg	1.04 ± 0.04	1.06 ± 0.08	1.01 ± 0.11
$G_{0.1}$, au/mmHg	1.15 ± 0.11	1.16 ± 0.14	1.35 ± 0.13
G_1, au/mmHg	2.73 ± 0.21	3.41 ± 0.51	4.84 ± 0.64††
G_{slope}, dB/decade	10.1 ± 1.0	10.4 ± 1.1	13.2 ± 0.8†
S_{10}, au/mmHg	−0.81 ± 0.03	−0.79 ± 0.05	−0.79 ± 0.11
S_{peak}, au/mmHg	−2.22 ± 0.15	−2.71 ± 0.35	−3.60 ± 0.40††
T_{peak}, s	0.37 ± 0.03	0.33 ± 0.02	0.35 ± 0.02
Peripheral arc			
$G_{0.01}$, mmHg/au	0.75 ± 0.07	0.79 ± 0.14	0.79 ± 0.14
$G_{0.1}$, mmHg/au	0.35 ± 0.05	0.48 ± 0.14	0.45 ± 0.12
G_1, mmHg/au	0.014 ± 0.008	0.008 ± 0.002	0.008 ± 0.003
G_{slope}, dB/decade	−34.0 ± 1.2	−31.4 ± 1.0	−32.8 ± 1.3
S_{50}, mmHg/au	0.89 ± 0.06	0.85 ± 0.15	0.81 ± 0.15
S_{slope}, mmHg·au^{-1}·s^{-1}	0.14 ± 0.01	0.20 ± 0.05	0.18 ± 0.05
Total baroreflex			
$G_{0.01}$, mmHg/mmHg	0.91 ± 0.08	0.84 ± 0.13	0.83 ± 0.11
$G_{0.1}$, mmHg/mmHg	0.41 ± 0.06	0.53 ± 0.09	0.58 ± 0.10
G_1, mmHg/mmHg	0.023 ± 0.009	0.025 ± 0.005	0.034 ± 0.006
G_{slope}, dB/decade	−24.6 ± 1.3‡‡	−22.3 ± 1.3‡‡	−19.8 ± 1.3‡‡
S_{50}, mmHg/mmHg	−1.03 ± 0.10	−0.85 ± 0.08	−0.83 ± 0.08
S_{slope}, mmHg·mmHg^{-1}·s^{-1}	−0.20 ± 0.02	−0.28 ± 0.04	−0.32 ± 0.05
HR control			
$G_{0.01}$, bpm/mmHg	0.46 ± 0.05	0.22 ± 0.04**	0.27 ± 0.05
$G_{0.1}$, bpm/mmHg	0.11 ± 0.01	0.04 ± 0.01**	0.08 ± 0.02†
S_{50}, bpm/mmHg	−0.52 ± 0.07	−0.18 ± 0.04**	−0.23 ± 0.05
S_{slope}, bpm·mmHg^{-1}·s^{-1}	−0.050 ± 0.004	−0.025 ± 0.005**	−0.036 ± 0.009

Data are presented as means ± SE ($n = 7$ for WKY and $n = 6$ for SHR). $G_{0.01}$, $G_{0.1}$, and G_1, dynamic gain values at 0.01, 0.1, and 1 Hz, respectively; G_{slope}, slope of dynamic gain between 0.1 and 1 Hz; S_{50}, steady-state response at 50 s; S_{peak}, peak response; S_{slope}, initial slope; S_{10}, step response at 10 s; T_{peak}, time to the negative peak. **$P < 0.01$ WKY_{120} vs. SHR_{120} by unpaired-*t*-test with Bonferroni correction. ††$P < 0.01$ and †$P < 0.05$, SHR_{120} versus SHR_{160} by paired-*t*-test with Bonferroni correction. ‡‡$P < 0.01$, peripheral arc versus total baroreflex by paired-*t*-test in each group.

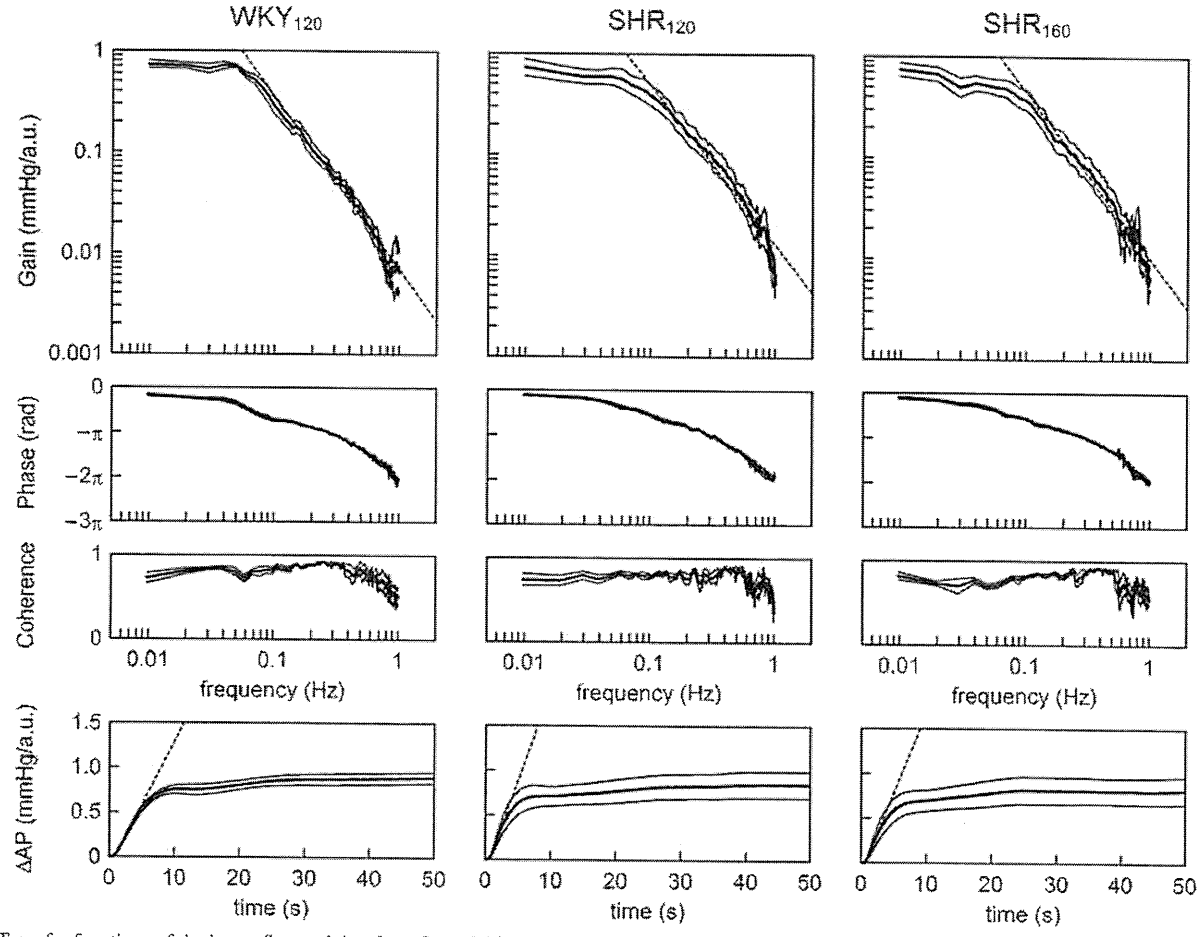

Fig. 3. Transfer functions of the baroreflex peripheral arc from SNA to AP averaged for WKY_{120}, SHR_{120} and SHR_{160} groups. Gain, phase, and coherence plots are shown. The dashed oblique line in the gain plot indicates G_{slope}. There is no significant difference in G_{slope} between WKY_{120} and SHR_{120} or between SHR_{120} and SHR_{160}. *Bottom*: step responses of AP calculated from the corresponding peripheral arc transfer functions. The dashed oblique line in the step response indicates the initial slope (S_{slope}) of the step response. There were no significant differences in S_{slope}. In all panels, the bold and thin lines indicate mean and mean ± SE values, respectively.

The total baroreflex transfer functions are depicted in Fig. 4. In the gain plots, the dynamic gain declined as the frequency increased above 0.05 Hz, indicating low-pass characteristics of the AP response to the CSP input. $G_{0.01}$, $G_{0.1}$, G_1, and G_{slope} did not differ significantly between WKY_{120} and SHR_{120} or between SHR_{120} and SHR_{160} (Table 2). The phase plots of three groups were also similar: the phase approached $-\pi$ radians at 0.01 Hz, reflecting the negative feedback operation attained by the total baroreflex. The phase was delayed as the frequency increased. For the step response, S_{50} and S_{slope} did not differ between WKY_{120} and SHR_{120} or between SHR_{120} and SHR_{160}. Within-group comparisons using paired *t*-test indicated that G_{slope} was significantly less negative in the total baroreflex than in the peripheral arc transfer function (Table 2).

The transfer functions from CSP to HR are shown in Fig. 5. In the gain plots, the dynamic gain decreased as the frequency increased. $G_{0.01}$ and $G_{0.1}$ were significantly smaller in SHR_{120} than in WKY_{120} (Table 2). Although $G_{0.01}$ did not differ between SHR_{120} and SHR_{160}, $G_{0.1}$ was significantly greater in SHR_{160} than in SHR_{120}. G_1 was not compared because coherence near zero and the phase with increased scatter suggested poor reliability of the estimated transfer functions above 0.8 Hz. In the phase plots, the phase approached $-\pi$ radians at 0.01 Hz, indicating that HR responded negatively to the CSP input. For the step responses, both S_{50} and S_{slope} were significantly less negative in SHR_{120} than in WKY_{120}, while S_{50} and S_{slope} did not differ significantly between SHR_{120} and SHR_{160}.

When the carotid sinus baroreflex was virtually closed by adjusting CSP to AP, mean AP (and thus mean CSP) in WKY was close to 120 mmHg and that in SHR was near 160 mmHg (Table 3). The mean HR and SNA in WKY under the baroreflex closed-loop conditions, however, seemed higher than those observed in WKY_{120}. Similarly, the mean HR and SNA in SHR seemed higher than those observed in SHR_{160}.

Data obtained from the supplemental protocol were summarized in Fig. 6 and Table 4. The gray lines indicate transfer functions derived from $WKY_{120\text{-}S}$, while the black lines indicate those derived from $WKY_{160\text{-}S}$. In the neural arc transfer function, dynamic gain values below 0.1 Hz tended to be lower in $WKY_{160\text{-}S}$ than in $WKY_{120\text{-}S}$. G_{slope} did not differ between $WKY_{120\text{-}S}$ and $WKY_{160\text{-}S}$. In the neural arc step response, S_{peak} did not differ significantly, and S_{10} was marginally attenuated in $WKY_{160\text{-}S}$ ($P = 0.06$). In the peripheral arc, parameters of the transfer function did not differ statistically between

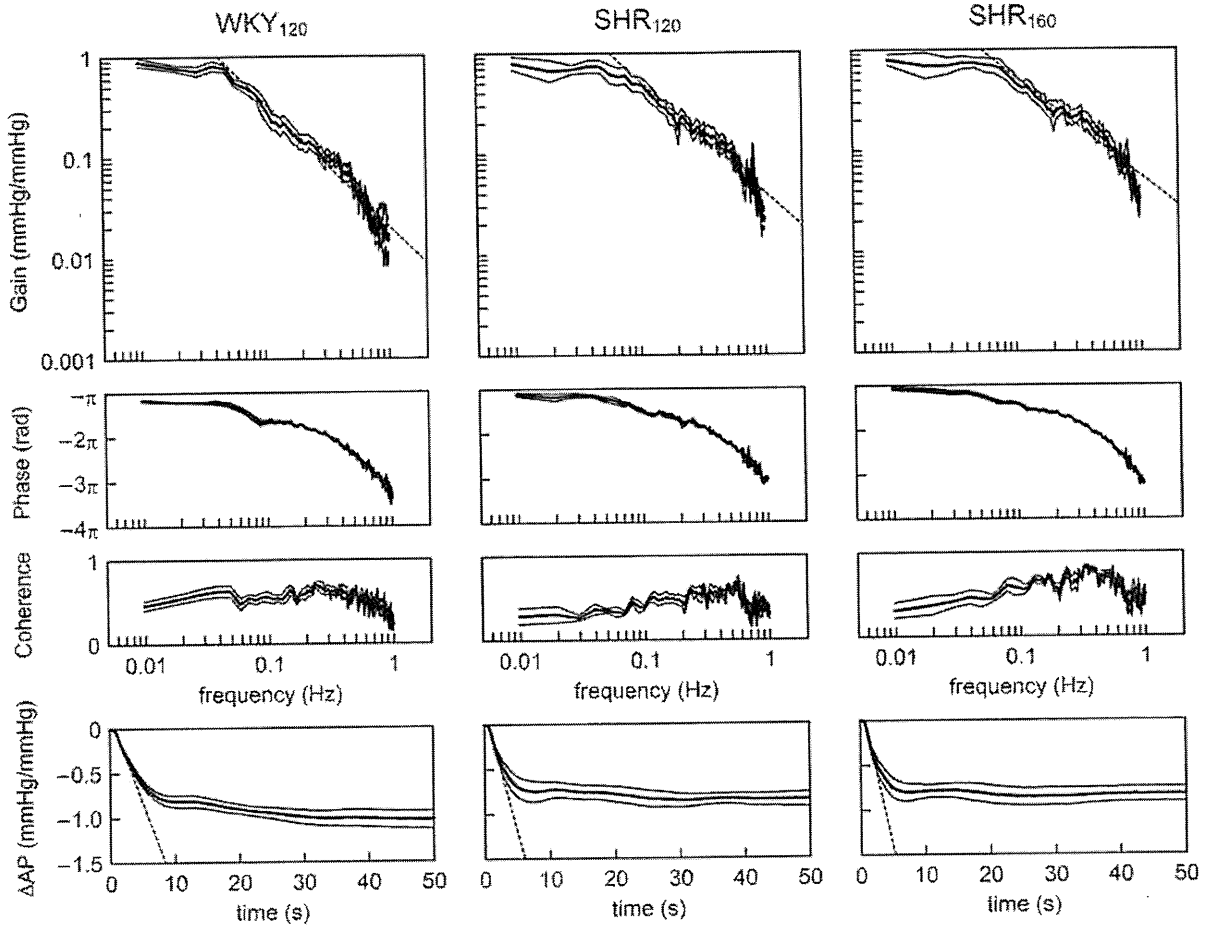

Fig. 4. Transfer functions of the total baroreflex from CSP to AP averaged for WKY_{120}, SHR_{120}, and SHR_{160} groups. Gain, phase, and coherence plots are shown. The dashed oblique line in the gain plot indicates G_{slope}. There is no significant difference in G_{slope} between WKY_{120} and SHR_{120} or between SHR_{120} and SHR_{160}. *Bottom*: step responses of AP calculated from the corresponding total baroreflex transfer functions. The dashed oblique line in the step response indicates the S_{slope}. There were no significant differences in S_{slope}. In all panels, the bold and thin lines indicate mean and mean ± SE values, respectively.

$WKY_{120\text{-}S}$ and $WKY_{160\text{-}S}$. In the peripheral arc step response, S_{slope} was significantly gentler in $WKY_{160\text{-}S}$. In the total baroreflex, although parameters of the transfer function did not differ statistically between $WKY_{120\text{-}S}$ and $WKY_{160\text{-}S}$, parameters of the step response, S_{50} and S_{slope}, were significantly attenuated in $WKY_{160\text{-}S}$.

DISCUSSION

In the present study, we comprehensively identified the open-loop transfer functions of the neural arc, peripheral arc, and total baroreflex in SHR using the normotensive WKY as a reference. Despite significant resetting of the baroreflex, the dynamic characteristics of AP regulation in SHR were comparable to those of WKY, except for a slight augmentation of the derivative characteristics of the neural arc at higher pressure input in SHR. On the other hand, the transfer function related to sympathetic HR control was significantly depressed in SHR compared with WKY.

Neural arc transfer function in SHR. The neural arc transfer function showed derivative characteristics in both WKY and SHR (Fig. 2), consistent with the findings of Harada et al. (7). The present results, however, differ slightly from the previous report in the following aspect. We demonstrated that G_1 and G_{slope} were significantly greater, and S_{peak} was significantly more negative in SHR_{160} than in SHR_{120}, indicating that higher pressure input enhanced the derivative characteristics in SHR. This was not simply an effect of the higher pressure input, because the higher pressure input did not increase G_1, G_{slope}, or S_{peak} in WKY (Fig. 6).

Both mechanosensory transduction at baroreceptors and central processing from baroreceptor afferent nerve activity to efferent SNA contribute to the generation of the derivative characteristics of the neural arc (16). According to a study by Brown et al. (1), the frequency response characteristics of aortic nerve discharge are similar between WKY and SHR in the frequency range of 0.1 to 20 Hz. Although direct comparison is difficult, the present results seem to be in line with their findings. Despite significant resetting in the static characteristics (24), dynamic characteristics of the carotid sinus baroreceptor transduction may not change appreciably in SHR.

Peripheral arc transfer function in SHR. There were no significant differences in the parameters of the peripheral arc transfer function between WKY and SHR (Fig. 3 and Table 2). A major neurotransmitter at the sympathetic nerve

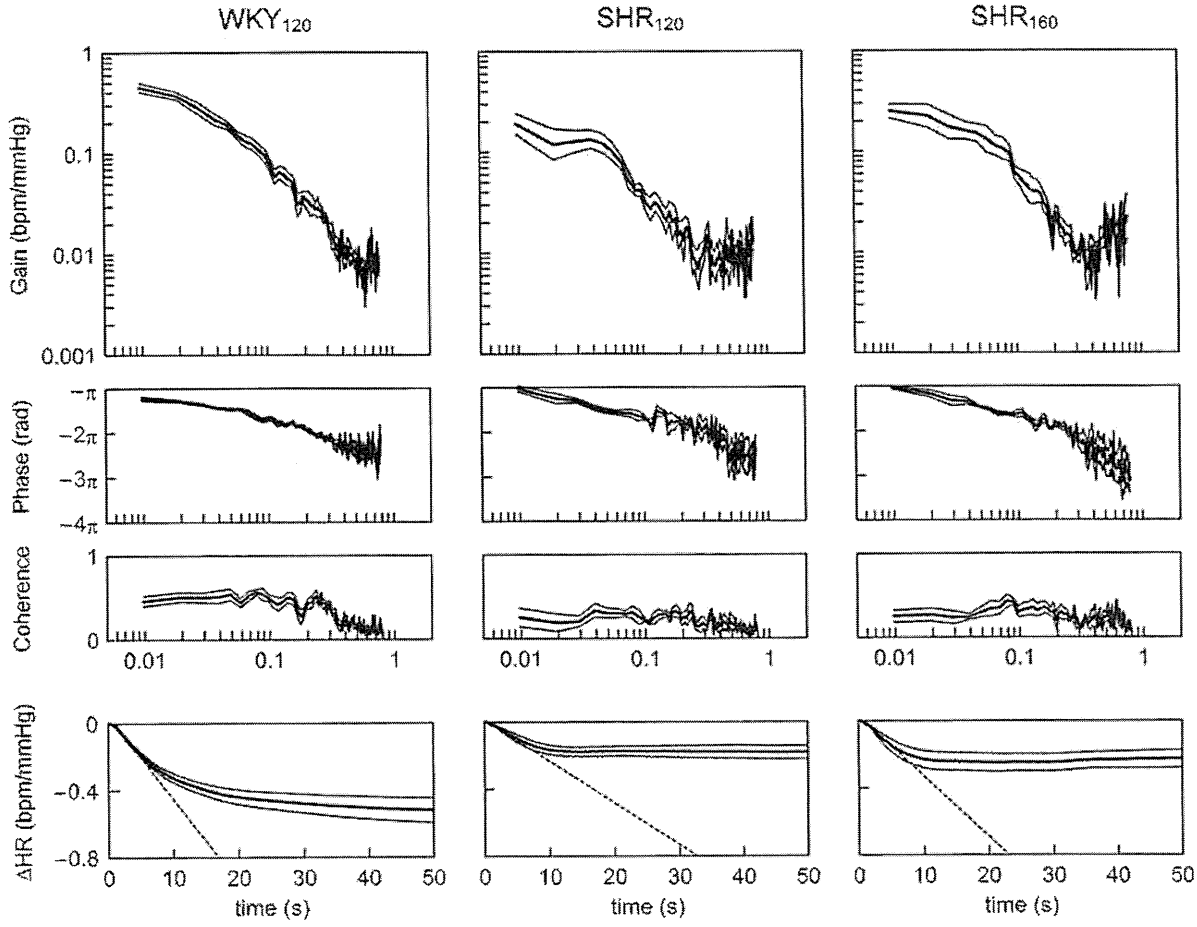

Fig. 5. Transfer functions from CSP to HR averaged for WKY_{120}, SHR_{120}, and SHR_{160} groups. Gain, phase, and coherence plots are shown. The dynamic gain values at 0.01 and 0.1 Hz are significantly smaller in SHR_{120} than in WKY_{120}. *Bottom*: step responses of HR calculated from the corresponding transfer functions. The dashed oblique line in the step response indicates S_{slope}. The steady-state step response and S_{slope} are significantly attenuated in SHR_{120} compared with WKY_{120}. In all panels, the bold and thin lines indicate mean and mean ± SE values, respectively.

endings is norepinephrine. The peripheral arc transfer function may thus reflect the combined dynamic properties of norepinephrine kinetics at the neuroeffector junction and the effector response to adrenergic stimulation (13). Neuronal uptake and α-adrenergic autoinhibition of norepinephrine operate to the same extent during electrical stimulation of the spinal cord in both SHR and WKY (36). Although norepinephrine uptake abnormalities have been reported in SHR (27, 28), the present results indicate that in this model, the influence of altered norepinephrine kinetics on the overall dynamic characteristics of the peripheral arc may be limited.

Table 3. *Mean AP, HR, and SNA under conditions of virtually closed baroreflex*

	WKY	SHR
Mean AP, mmHg	121 ± 3	156 ± 5**
Mean HR, bpm	414 ± 16	433 ± 13
Mean SNA, au	103 ± 14	130 ± 18

Data are presented in means ± SE (n = 7 for WKY and n = 6 for SHR). bpm, beats per minute; au, arbitrary unit. **P < 0.01 by unpaired-t-test.

In pithed rats, pressor response to electrical stimulation of the spinal cord is greater in SHR than in WKY (21, 36). Pressor response to norepinephrine or epinephrine is also enhanced in SHR (36). While the maximum pressor response to methoxamine is greater in SHR than in WKY, the pressor response to submaximal doses of methoxamine is attenuated in SHR (21). The present results suggest that the dynamic characteristics of the peripheral arc are not remarkably different between WKY and SHR despite possible differences in vascular sensitivity to adrenergic stimulation.

Total baroreflex transfer function in SHR. There were no significant differences in the parameters of the total baroreflex transfer function between WKY and SHR (Fig. 4, Table 2), even though AP was significantly higher in SHR than in WKY. In contrast, the step response of the total baroreflex was significantly attenuated in $WKY_{160\text{-}S}$ than in $WKY_{120\text{-}S}$ (Fig. 6, Table 4), indicating that the preservation of the total baroreflex function at the higher pressure input may be unique to SHR. In each of the WKY_{120}, SHR_{120}, and SHR_{160} groups, G_{slope} was significantly less negative in the total baroreflex than in the corresponding peripheral arc, suggesting an improvement of dynamic gain in the higher-frequency range of 0.1 to 1 Hz. The

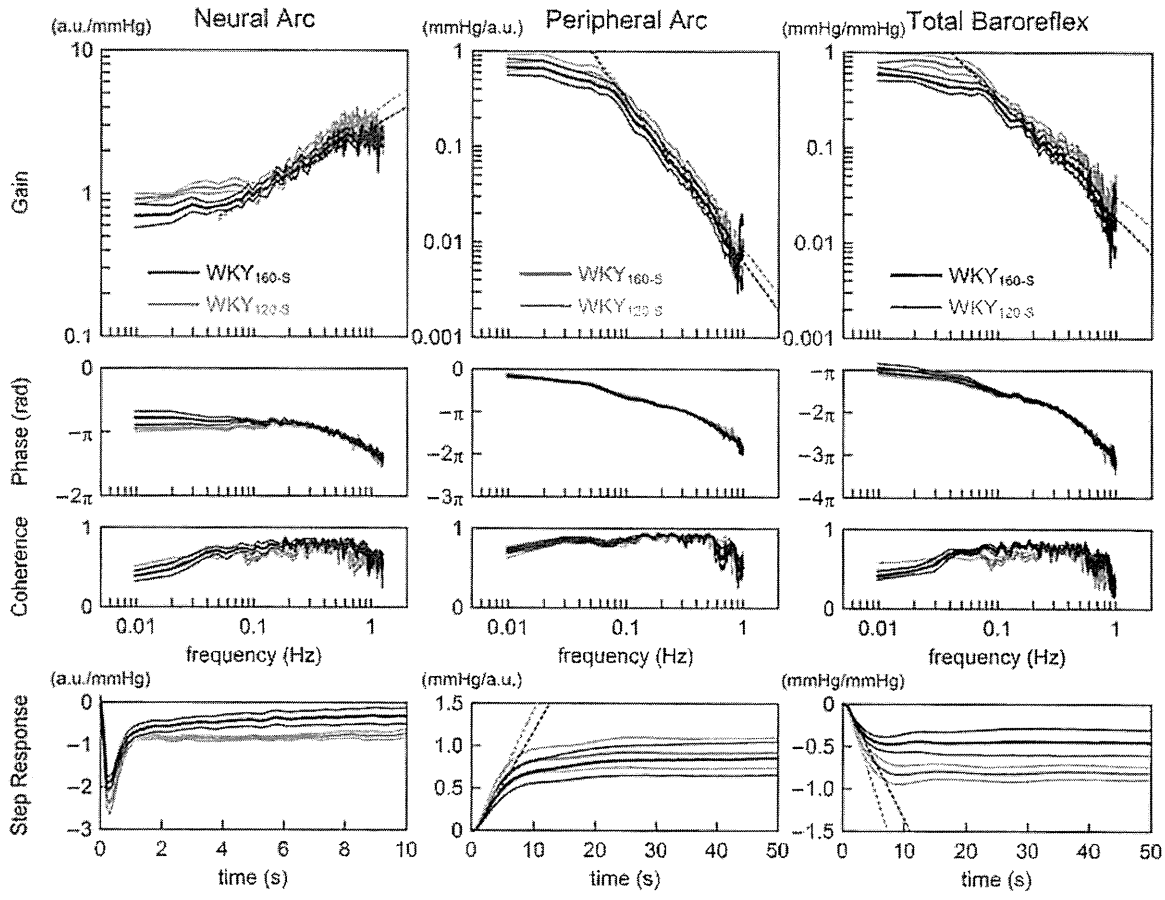

Fig. 6. Transfer functions of the neural arc, peripheral arc, and total baroreflex obtained from an additional protocol. In each panel, the gray lines indicate the transfer functions estimated from $WKY_{120\text{-}S}$. The black lines indicate the transfer functions estimated from $WKY_{160\text{-}S}$. No significant enhancement at the higher pressure input was observed in the derivative characteristics of the neural arc transfer function between 0.1 and 1 Hz. *Bottom*: step responses corresponding to the respective transfer functions. S_{slope} in the peripheral arc was significantly gentler in $WKY_{160\text{-}S}$ than in $WKY_{120\text{-}S}$. Both S_{50} and S_{slope} in the total baroreflex were significantly attenuated in $WKY_{160\text{-}S}$ than in $WKY_{120\text{-}S}$. In all panels, the bold and thin lines indicate mean and mean ± SE values, respectively.

neural arc may thus serve as an accelerating mechanism to improve the dynamic AP regulation in both WKY and SHR. Because G_{slope} in the neural arc was significantly greater in SHR_{160} than in SHR_{120} and G_{slope} in the peripheral arc did not differ between the two groups, G_{slope} in the total loop is expected to be less negative in SHR_{160}. This difference was not detected statistically, however, probably because an increase of G_{slope} by 2.4 dB/decade in the neural arc was partially offset by a decrease of G_{slope} by 1.4 dB/decade in the peripheral arc.

The well-preserved total baroreflex transfer function in SHR is in marked contrast to the significant depression of total baroreflex transfer function in chronic heart failure rats after myocardial infarction (12). Osborn (26) has demonstrated that sinoaortic denervation does not chronically increase mean AP in SHR, suggesting that the arterial baroreflex does not contribute much to the chronic regulation of mean AP in SHR. Nevertheless, the present results imply that the arterial baroreflex in SHR is still important for attenuating acute disturbances in AP.

Transfer function of HR control. In contrast to the total baroreflex transfer function, the transfer function of HR control showed significant depression in dynamic gain in SHR. Although the decreased baroreflex-mediated HR response is primarily attributed to a defect in parasympathetic control (29), the present results obtained in vagotomized rats indicate that the dynamic sympathetic control of HR may also be depressed in SHR. Despite the significant alteration in the sympathetic HR control, the total baroreflex transfer function did not differ between WKY and SHR, suggesting little contribution of HR to the determination of dynamic AP regulation. The lack of significant effect of HR on the dynamic AP regulation is consistent with the findings in rabbits (13, 25).

Baroreflex closed-loop conditions. In the present experimental settings, the baroreflex could be virtually closed by adjusting CSP to AP. The closed-loop operating AP (Table 3) provides a rationale for the selection of the mean input pressure of CSP. When CSP was perturbed around the operating-point pressure, however, mean SNA and AP usually decreased (10). The phenomenon may be related to the input pulsatility and the effect of input amplitude (3, 17, 35). Mean SNA and AP are expected to decrease as the input amplitude of CSP perturbation increases when the mean CSP is lower than the midpoint of the inverse sigmoidal curve characterizing the CSP-SNA relationship.

Table 4. *Parameters of estimated transfer functions and step responses in an additional protocol*

	$WKY_{120\text{-}S}$	$WKY_{160\text{-}S}$
Neural arc		
$G_{0.01}$, au/mmHg	0.93 ± 0.07	0.76 ± 0.14
$G_{0.1}$, au/mmHg	1.08 ± 0.13	1.02 ± 0.09
G_1, au/mmHg	3.12 ± 0.34	2.74 ± 0.25
G_{slope}, dB/decade	11.4 ± 1.2	9.6 ± 0.8
S_{10}, au/mmHg	−0.77 ± 0.09	−0.32 ± 0.19
S_{peak}, au/mmHg	−2.41 ± 0.25	−1.97 ± 0.16
T_{peak}, s	0.35 ± 0.02	0.36 ± 0.03
Peripheral arc		
$G_{0.01}$, mmHg/au	0.83 ± 0.17	0.76 ± 0.17
$G_{0.1}$, mmHg/au	0.35 ± 0.07	0.33 ± 0.08
G_1, mmHg/au	0.025 ± 0.015	0.030 ± 0.017
G_{slope} , dB/decade	−32.1 ± 1.0	−33.7 ± 1.2
S_{50}, mmHg/au	0.92 ± 0.18	0.85 ± 0.20
S_{slope}, mmHg·au^{-1}·s^{-1}	0.15 ± 0.03	0.13 ± 0.03**
Total baroreflex		
$G_{0.01}$, mmHg/mmHg	0.88 ± 0.19	0.63 ± 0.08
$G_{0.1}$, mmHg/mmHg	0.39 ± 0.06	0.35 ± 0.06
G_1, mmHg/mmHg	0.022 ± 0.009	0.042 ± 0.022
G_{slope}, dB/decade	−21.6 ± 0.9	−24.8 ± 1.6
S_{50}, mmHg/mmHg	−0.81 ± 0.08	−0.45 ± 0.15*
S_{slope} , mmHg·mmHg^{-1}·s^{-1}	−0.22 ± 0.03	−0.14 ± 0.04*

Data are presented as means ± SE (n = 6 data sets from 3 rats). *P < 0.05 and **P < 0.01 by paired t-test.

Limitation. First, we performed the experiments in anesthetized rats, which might have affected the estimation of baroreflex function. However, since we compared the baroreflex dynamic characteristics between WKY and SHR under the same anesthetic procedures, the interpretations of the present results may be reasonable. Second, although we examined splanchnic SNA as a representative of systemic SNA, the dynamic characteristics of SNA response could vary in different neural districts (15). Nevertheless, the derivative characteristics of the neural arc in SHR were also evident even when renal SNA was evaluated (7). Third, we occluded the common carotid arteries to isolate the carotid sinuses. Although the vertebral arteries were preserved, we cannot rule out the possibility that the carotid occlusion might have affected the present results. Finally, we transected the vagal nerves to obtain baroreflex open-loop conditions. Further studies are needed to clarify the role of the vagal system in dynamic cardiovascular regulation. Especially, the dynamic HR control may vary greatly in the presence or absence of the vagal efferent nerves (22).

In summary, the neural arc transfer function retained the derivative characteristics in SHR. The peripheral arc and total baroreflex transfer function did not differ significantly between SHR and WKY, suggesting that dynamic AP regulation was well preserved in SHR. In contrast, the dynamic sympathetic HR control seemed significantly attenuated in SHR compared with WKY.

Perspectives and Significance

The arterial baroreflex has been considered to play a minor role in the long-term AP regulation, since denervation of baroreceptor-afferent fibers does not result in a long-lasting hypertension (4, 6). Recent findings, however, indicate that the stimulation of baroreceptor afferent fibers may reduce SNA and AP for a longer period (19). A carotid baroreceptor stimulator has been explored as an alternative therapy for multiple drug-resistant hypertension (8). The device, however, does not seem to take the dynamic characteristics of AP regulation into account and delivers a prescribed stimulation. Ideally, such devices should be activated on a necessary basis, i.e., depressor and pressor function should operate only in the face of hypertensive and hypotensive events, respectively. Understanding of the dynamic characteristics of AP regula-

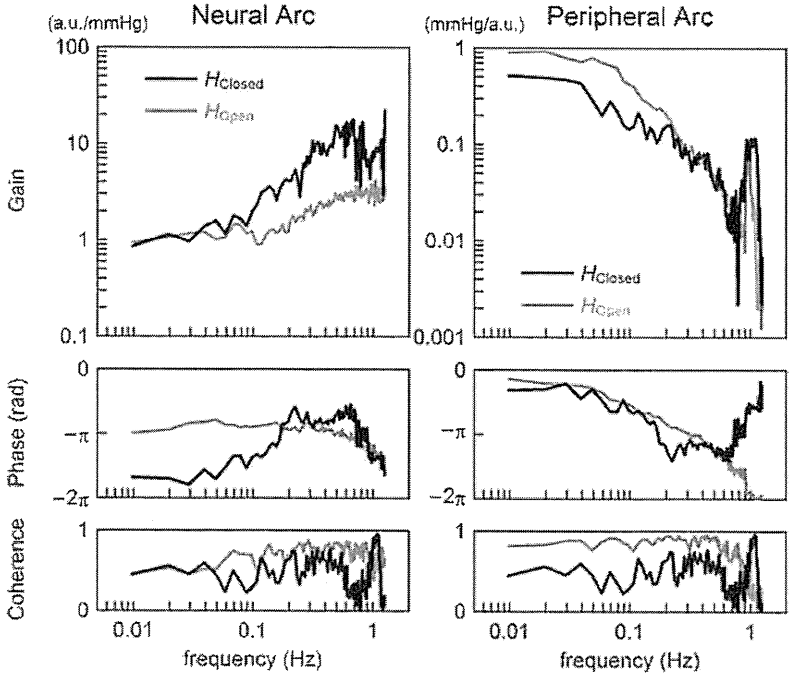

Fig. 7. Comparison of the transfer functions estimated using open-loop data with an exogenous perturbation (gray lines, H_{Open}) and those estimated using closed-loop baseline data without exogenous perturbations (black lines, H_{Closed}) in the same rat. The transfer functions estimated using closed-loop baseline data do not usually extract the dynamic characteristics of the baroreflex neural and peripheral arcs precisely (see APPENDIX for details).

tion in physiological and pathological conditions will contribute to designing an intelligent controller system of such devices (14, 33).

APPENDIX

Consideration on open-loop systems analysis. If a standard transfer function analysis is applied to closed-loop baseline data without exogenous perturbations, the resultant transfer function cannot usually extract open-loop system characteristics precisely. Fig. 7 represents neural and peripheral arc transfer functions estimated using open-loop data with an exogenous CSP input (the gray lines, H_{Open}) and those estimated using closed-loop baseline data without exogenous perturbations (the black lines, H_{Closed}) in the same rat. In the gain plot of the neural arc, although H_{Closed} reveals derivative characteristics, they are much more exaggerated than those seen in H_{Open}. The phase plot of H_{Closed} does not reflect the inverse relation between CSP and SNA below 0.1 Hz. In the gain plot of the peripheral arc, dynamic gain values below 0.2 Hz are smaller in H_{Closed} than in H_{Open}. Although the phase plots are similar between H_{Closed} and H_{Open}, they are dissociated, for instance, at around 0.2 Hz. The phase plots of H_{Closed} are mathematically reversed, and the coherence plots of H_{Closed} are mathematically identical between the neural and peripheral arcs. To what extent H_{Closed} resembles H_{Open} critically depends on the property and magnitude of inherent noise under a given condition, which is usually unknown.

Whiteness of an input signal is prerequisite to estimate a system open-loop transfer function as follows. Take the estimation of a neural arc transfer function, for example. SNA can be expressed in the frequency domain as

$$SNA(f) = H_N(f)CSP(f) + N(f) \qquad (A1)$$

where $SNA(f)$, $CSP(f)$, and $N(f)$ denote Fourier transforms of SNA, CSP, and inherent central noise that is unknown. $H_N(f)$ represents the neural arc transfer function. Calculating cross-spectral densities between terms of *Eq. A1* and $CSP(f)$ and performing ensemble averages, we have

$$E[SNA(f)CSP(f)^*] = H_N(f)E[CSP(f)CSP(f)^*] + E[N(f)CSP(f)^*] \qquad (A2)$$

where $CSP(f)^*$ indicates a complex conjugate of $CSP(f)$. Because the system characteristics are supposed to be time invariant, $H_N(f)$ can be outside the operation of ensemble average, $E[...]$. The last term $E[N(f)CSP(f)^*]$ asymptotically diminishes when CSP is white noise, because the white noise is statistically independent of other signals. Therefore, $H_N(f)$ can be estimated as follows:

$$H_N(f) = \frac{E[SNA(f)CSP(f)^*]}{E[CSP(f)CSP(f)^*]} \qquad (A3)$$

Note that the inherent noise in SNA can affect AP through the baroreflex peripheral arc. Under baroreflex closed-loop conditions, CSP is inevitably influenced by AP and thus by the inherent noise in SNA. In other words, $N(f)$ and $CSP(f)$ are no longer independent once the baroreflex is closed. In this situation, $H_N(f)$ has to be calculated as

$$H_N(f) = \frac{E[SNA(f)CSP(f)^*] - E[N(f)CSP(f)^*]}{E[CSP(f)CSP(f)^*]} \qquad (A4)$$

Applying *Eq. A3* instead of *Eq. A4* is one of the reasons for the dissociation between H_{Closed} and H_{Open}. Unfortunately, *Eq. A4* cannot be used ordinarily for analyzing the closed-loop data because $N(f)$ is unknown.

Another important issue is that *Eq. A3* can be ill posed if the denominator is close to zero. In other words, CSP needs to have sufficient power spectral densities at all the frequencies of interest. If there are no sufficient inputs at specific frequencies, there is no way to identify the system characteristics at those frequencies without any assumption or a priori knowledge about the system. The white noise input, which is rich in frequency components, meets the conditions required to stably solve the *Eq. A3*.

GRANTS

This study was supported by Health and Labour Sciences Research Grants (H18-nano-Ippan-003, H19-nano-Ippan-009, H20-katsudo-Shitei-007, and H21-nano-Ippan-005) from the Ministry of Health, Labour and Welfare of Japan; by a Grant-in-Aid for Scientific Research (No. 20390462) from the Ministry of Education, Culture, Sports, Science and Technology of Japan; and by the Industrial Technology Research Grant Program from the New Energy and Industrial Technology Development Organization of Japan.

DISCLOSURES

No conflicts of interest, financial or otherwise, are declared by the authors.

REFERENCES

1. **Brown AM, Saum WR, Yasui S.** Baroreceptor dynamics and their relationship to afferent fiber type and hypertension. *Circ Res* 42: 694–702, 1978.
2. **Chapleau, MW.** Arterial baroreflexes. In: *Hypertension Primer* (4th ed), edited by Izzo JL Jr, Sica DA, and Black HR. Philadelphia, PA: Lippincott Williams & Wilkins, 2008, p. 120–123.
3. **Chapleau MW, Abboud FM.** Contrasting effects of static and pulsatile pressure on carotid baroreceptor activity in dogs. *Circ Res* 61: 648–658, 1987.
4. **Cowley AW Jr, Liard JF, Guyton AC.** Role of baroreceptor reflex in daily control of arterial blood pressure and other variables in dogs. *Circ Res* 32: 564–576, 1973.
5. **Glantz SA.** *Primer of Biostatistics* (5th ed). New York, NY: McGraw-Hill, 2002.
6. **Guyton AC, Coleman TG, Cowley AW Jr, Manning RD Jr, Norman RA Jr, Ferguson JD.** Brief reviews: A systems analysis approach to understanding long-range arterial blood pressure control and hypertension. *Circ Res* 35: 159–176, 1974.
7. **Harada S, Imaizumi T, Ando S, Hirooka Y, Sunagawa K, Takeshita A.** Arterial baroreflex dynamics in normotensive and spontaneously hypertensive rats. *Am J Physiol Regul Integr Comp Physiol* 263: R524–R528, 1992.
8. **Heusser K, Tank J, Engeli S, Diedrich A, Menne J, Eckert S, Peters T, Sweep FC, Haller H, Pichlmaier AM, Luft FC, Jordan J.** Carotid baroreceptor stimulation, sympathetic activity, baroreflex function, and blood pressure in hypertensive patients. *Hypertension* 55: 619–626, 2010.
9. **Ikeda Y, Kawada T, Sugimachi M, Kawaguchi O, Shishido T, Sato T, Miyano H, Matsuura W, Alexander J Jr, Sunagawa K.** Neural arc of baroreflex optimizes dynamic pressure regulation in achieving both stability and quickness. *Am J Physiol Heart Circ Physiol* 271: H882–H890, 1996.
10. **Kashihara K, Takahashi Y, Chatani K, Kawada T, Zheng C, Li M, Sugimachi M, Sunagawa K.** Intravenous angiotensin II does not affect dynamic baroreflex characteristics of the neural or peripheral arc. *Jpn J Physiol* 53: 135–143, 2003.
11. **Kawada T, Kamiya A, Li M, Shimizu S, Uemura K, Yamamoto H, Sugimachi M.** High levels of circulating angiotensin II shift the open-loop baroreflex control of splanchnic sympathetic nerve activity, heart rate and arterial pressure in anesthetized rats. *J Physiol Sci* 59: 447–455, 2009.
12. **Kawada T, Li M, Kamiya A, Shimizu S, Uemura K, Yamamoto H, Sugimachi M.** Open-loop dynamic and static characteristics of the carotid sinus baroreflex in rats with chronic heart failure after myocardial infarction. *J Physiol Sci* 60: 283–298, 2010.
13. **Kawada T, Miyamoto T, Uemura K, Kashihara K, Kamiya A, Sugimachi M, Sunagawa K.** Effects of neuronal norepinephrine uptake blockade on baroreflex neural and peripheral arc transfer characteristics. *Am J Physiol Regul Integr Comp Physiol* 286: R1110–R1120, 2004.
14. **Kawada T, Shimizu S, Yamamoto H, Shishido T, Kamiya A, Miyamoto T, Sunagawa K, Sugimachi M.** Servo-controlled hind-limb electrical stimulation for short-term arterial pressure control. *Circ J* 73: 851–859, 2009.
15. **Kawada T, Shishido T, Inagaki M, Tatewaki T, Zheng C, Yanagiya Y, Sugimachi M, Sunagawa K.** Differential dynamic baroreflex regulation

of cardiac and renal sympathetic nerve activities. *Am J Physiol Heart Circ Physiol* 280: H1581–H1590, 2001.
16. **Kawada T, Yamamoto K, Kamiya A, Ariumi H, Michikami D, Shishido T, Sunagawa K, Sugimachi M.** Dynamic characteristics of carotid sinus pressure-nerve activity transduction in rabbits. *Jpn J Physiol* 55: 157–163, 2005.
17. **Kawada T, Yanagiya Y, Uemura K, Miyamoto T, Zheng C, Li M, Sugimachi M, Sunagawa K.** Input-size dependence of the baroreflex neural arc transfer characteristics. *Am J Physiol Heart Circ Physiol* 284: H404–H415, 2003.
18. **Kawada T, Sugimachi M, Sato T, Miyano H, Shishido T, Miyashita H, Yoshimura R, Takaki H, Alexander J Jr, Sunagawa K.** Closed-loop identification of carotid sinus baroreflex open-loop transfer characteristics. *Am J Physiol Heart Circ Physiol* 273: H1024–H1031, 1997.
19. **Lohmeier TE, Iliescu R, Dwyer TM, Irwin ED, Cates AW, Rossing MA.** Sustained suppression of sympathetic activity and arterial pressure during chronic activation of the carotid baroreflex. *Am J Physiol Heart Circ Physiol* 299: H402–H409, 2010.
20. **Marmarelis PZ, Marmarelis VZ.** The white noise method in system identification. In: *Analysis* of Physiological Systems. New York: Plenum, 131–180, 1978.
21. **Mills E, Bruckert JW.** Pressor mechanisms linked obligatorily to spontaneous hypertension in the rat. *Hypertension* 11: 427–432, 1988.
22. **Mizuno M, Kawada T, Kamiya A, Miyamoto T, Shimizu S, Shishido T, Smith SA, Sugimachi M.** Dynamic characteristics of heart rate control by the autonomic nervous system in rats. *Exp Physiol* 95: 919–925, 2010.
23. **Mohrman DE, Heller LJ.** *Cardiovascular Physiology* **(6th ed).** New York: McGraw Hill, 2006, p. 172–177. 2006.
24. **Nosaka S, Wang SC.** Carotid sinus baroreceptor functions in the spontaneously hypertensive rat. *Am J Physiol* 222: 1079–1084, 1972.
25. **Liu HK, Guild SJ, Ringwood JV, Barrett CJ, Leonard BL, Nguang SK, Navakatikyan MA, Malpas SC.** Dynamic baroreflex control of blood pressure: influence of the heart vs. peripheral resistance. *Am J Physiol Regul Integr Comp Physiol* 283: R533–R542, 2002.
26. **Osborn JW.** Pathogenesis of hypertension in the sinoaortic-denervated spontaneously hypertensive rat. *Hypertension* 18: 475–482, 1991.
27. **Rho JH, Newman B, Alexander N.** Altered in vitro uptake of norepinephrine by cardiovascular tissues of spontaneously hypertensive rats. Part 1. In: *Mesenteric Artery Hypertension* 3: 704–709, 1981.
28. **Rho JH, Newman B, Alexander N.** Altered in vitro uptake of norepinephrine by cardiovascular tissues of spontaneously hypertensive rats. Part 2. Portal-mesenteric veins and atria. *Hypertension* 3: 710–717, 1981.
29. **Salgado HC, Barale AR, Castania JA, Machado BH, Chapleau MW, Fazan R Jr.** Baroreflex responses to electrical stimulation of aortic depressor nerve in conscious SHR. *Am J Physiol Heart Circ Physiol* 292: H593–H600, 2007.
30. **Sapru HN, Wang SC.** Modification of aortic baroreceptor resetting in the spontaneously hypertensive rat. *Am J Physiol* 230: 664–674, 1976.
31. **Sato T, Kawada T, Inagaki M, Shishido T, Sugimachi M, Sunagawa K.** Dynamics of sympathetic baroreflex control of arterial pressure in rats. *Am J Physiol Regul Integr Comp Physiol* 285: R262–R270, 2003.
32. **Sato T, Kawada T, Miyano H, Shishido T, Inagaki M, Yoshimura R, Tatewaki T, Sugimachi M, Alexander J Jr, Sunagawa K.** New simple methods for isolating baroreceptor regions of carotid sinus and aortic depressor nerves in rats. *Am J Physiol Heart Circ Physiol* 276: H326–H332, 1999.
33. **Sato T, Kawada T, Sugimachi M, Sunagawa K.** Bionic technology revitalizes native baroreflex function in rats with baroreflex failure. *Circulation* 106: 730–734, 2002.
34. **Shoukas AA, Callahan CA, Lash JM, Haase EB.** New technique to completely isolate carotid sinus baroreceptor regions in rats. *Am J Physiol Heart Circ Physiol* 260: H300–H303, 1991.
35. **Ursino M, Fiorenzi A, Belardinelli E.** The role of pressure pulsatility in the carotid baroreflex control: a computer simulation study. *Comput Biol Med* 26: 297–314, 1996.
36. **Yamaguchi I, Kopin IJ.** Blood pressure, plasma catecholamines, and sympathetic outflow in pithed SHR and WKY rats. *Am J Physiol Heart Circ Physiol* 238: H365–H372, 1980.